Journal of Electronics and Electrical Engineering
https://ojs.wiserpub.com/index.php/JEEE/

UNIVERSAL WISER PUBLISHER

Short Communication

Dual-Mode Dielectric Waveguide Monoblock Filter Design

Yahui Wu*, Lukui Jin, Zhenxiong Xie

Department of Research and Development, Anhui Tatfook Technology Co., Ltd., Shenzhen, 518104, China.
E-mail: wyhalbert@qq.com

Received: 25 July 2022; **Revised:** 23 September 2022; **Accepted:** 27 September 2022

Abstract: This paper presents a design of dielectric waveguide filter using dual-mode dielectric waveguide resonators (DWRs). The filter is formed by a ceramic monoblock, thus it is compact and ease of fabrication. The employed degenerate modes of DWR are TE_{101} and TE_{011} mode, which can be coupled by a slot on the dielectric block. The coupling between a dual-mode DWR and a single-mode DWR is realized by aperture and slot. The external coupling is realized by a silver-coated blind hole that aligns to the mode for excitation. Transmission zero (TZ) can be flexibly generated above or below passband, by changing the relative position of coupling slot. A sixth order bandpass filter working at 4.9 GHz is designed using dual- and single-mode DWRs. The filter is fabricated and measured, agreeing well with simulation. This filter has compact size, low insertion loss, good selectivity and wide spurious-free response, which is applicable to 5G base stations.

Keywords: dielectric resonator, dual-mode, bandpass filter

1. Introduction

Modern wireless communication system requires miniaturized RF components to reduce the size and weight of RF system. 5G communication system uses massive multiple-input-multiple-output (mMIMO) technology, which is realized by antenna arrays [1,2]. Consequently, the transmitting and receiving paths require compact filter solution to significantly reduce the size of 5G base stations. DWR filters, which are made of silver-coated ceramic block, have smaller size, less weight, and lower cost when compared to traditional metal cavity filters [3]. Single-mode DWR filters are now widely used in active antenna unit (AAU) of 5G base stations. Waveguide bandpass filters have been recently developed for W-band and THz applications.

Multi-mode air-filled waveguide filters [4,5,6,7] and metal cavity filters that use multi-mode dielectric resonators [8,9,10] have been reported. A filter was proposed in [11], cascading two triple-mode DWRs with a metal cavity coaxial resonator in between. These filters are based on air-filled metal cavities, resulting large size and weight.

In recent years, dual- and triple-mode dielectric cavity structures based on quasi-TEM modes have been studied [12,13]. The resonances are generated by quasi-quarter-wavelength blind holes in the dielectric cavity. Dual-mode DWRs based on a pair of TE_{201} modes, TM_{120} and TM_{210} modes have been proposed in [14] and [15]. The dual-mode is actually a combination of two single-mode resonators in a dielectric cavity. Besides, their unloaded Q-factors are relatively low because the degenerate modes are not used.

This paper presents a dielectric waveguide monoblock filter using dual-mode DWRs. The dual-mode DWR virtually saves up to 50% space with relatively high Q-factors, when compared to the volume of two single-mode

DOI: https://doi.org/10.37256/jeee.1120221681

DWRs. The inter-mode and inter-resonator coupling structures for proposed dual-mode DWRs are studied. Meanwhile, the generation of TZ for a DWR filter is analyzed. A sixth order bandpass filter that based on single- and dual-mode DWRs is designed, fabricated and tested. The filter has very good selectivity, contributed from two TZs at stopband. It is very compact, made of a silver-coated ceramic monoblock, which is ease of fabrication. The implemented filter is applicable to band N79 AAU of 5G base stations.

2. Resonator and Coupling Structures

2.1 *Resonator Design*

Figure 1 shows an ideal dual-mode DWR and the electric field distribution of TE_{101} and TE_{011} mode. The resonator is a silver-coated rectangular dielectric block with the following dimensions: ***L***=10.8 mm, ***W***=***H***=8.9 mm. The dielectric constant is 19.85 and loss tangent is 0.0002. The degenerate modes are resonating at 4.9 GHz, with E-fields aligning to Y-and X-axis, respectively.

Table 1 compares two single-TE-mode DWRs with the designed dual-mode DWR. A single-TE_{101}-mode DWR without cut-planes in [16] and a single-TE_{011}-mode [17] are redesigned to resonate at 4.9GHz. The resonators were EM simulated by Eigenmode Solver. The proposed dual- mode DWR offers 15% higher Q and 27% more space efficiency than the single-TE_{101}-mode resonator. It has 77% higher Q and 60% more space efficiency, in comparison with single-TE_{011}-mode resonator.

Blind holes are usually introduced at XZ and YZ planes for the frequency tuning of resonant modes. The tuning holes break the symmetry of the ideal dual-mode DWR, thus separate the frequencies of degenerate modes.

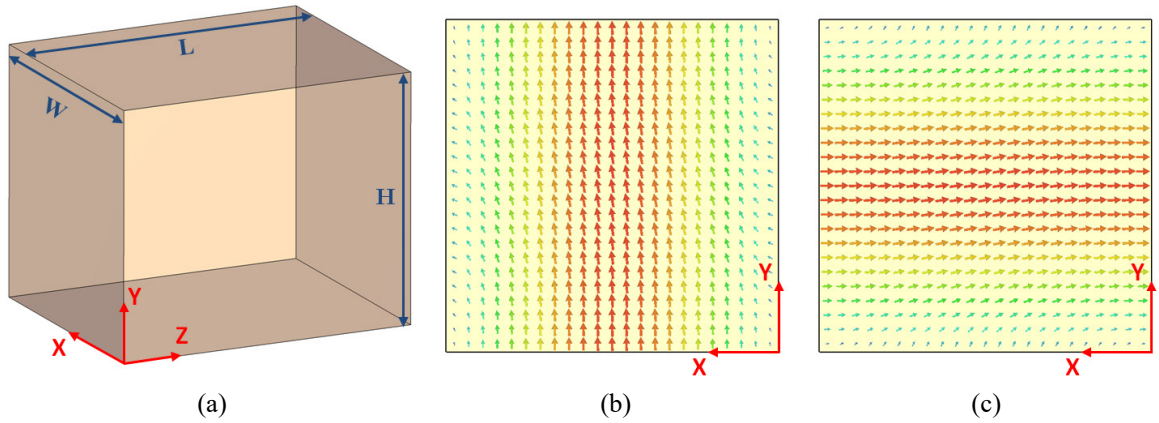

Figure 1. A dual-mode DWG resonator. (a) 3D structure. (b) E-field of TE_{101} mode. (c) E-field of TE_{011} mode.

Table 1. Comparison with Single-mode DWG Resonators

Resonator	[16]	[17]	This work
Resonant mode	TE_{101}	TE_{011}	TE_{101} and TE_{011}
No. of Modes (N)	1	1	2
Volume (mm^3)	9.7×9.7×5	8×8×6	8.9×8.9×10.8
Q-factor (Q)	1700	1100	1950
Space Efficiency (Q×N/V)	3.6	2.86	4.56

2.2 *Coupling Structures*

The coupling coefficients between resonant mode *m* and *n* are derived by

$$k_{mn} = \frac{f_m^{\ 2} - f_n^2}{f_m^2 + f_n^2} \tag{1}$$

where f_m and f_n represent the resonant frequency of mode *m* and *n*, respectively.

The degenerate TE_{101} and TE_{011} mode can be coupled by a silver-coated slot, as shown in Figure 2(a). The tuning holes are located at the center of XZ and YZ planes. The dimensions of resonator are as follows: $\boldsymbol{L}$=10.8 mm, $\boldsymbol{W}$=$\boldsymbol{H}$=8.8 mm and $\boldsymbol{D_0}$=1.5 mm. The depths of tuning holes are $\boldsymbol{H_1}$=$\boldsymbol{H_2}$=0.5 mm. Figure 2(b) shows the inter-mode coupling coefficient against slot dimensions, where mode 1 and 2 represents the original TE_{101} and TE_{011} mode, respectively. The tuning holes for dual-mode DWRs are relatively small to have negligible effect on separating the resonances and influencing inter-mode couplings.

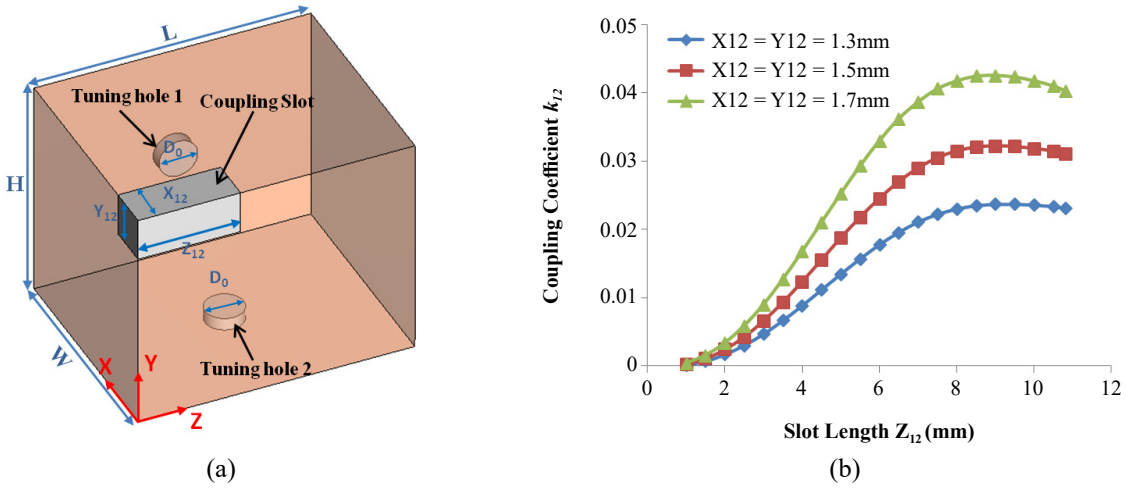

(a) (b)

Figure 2. Inter-mode coupling structure and coefficients. (a) Coupling structure. (b) Simulated coupling coefficients

Figure 3 shows a structure that cascades the designed dual-mode DWR with a single-TE_{101}-mode DWR. The TE_{101} mode of single-mode DWR is represented by mode 3. The tuning hole for single-TE_{101}-mode DWR is relatively large in radius so that it is consistent with current single-mode dielectric waveguide filters. It is also ease of fabrication and tuning to have a large blind hole for such size dielectric blocks. The coupling between mode 2 and 3 is realized and controlled by an aperture realized by dielectric, whereas mode 1 and 3 is coupled by a slot on the dual-mode DWR. Since the slot for k_{13} breaks the symmetry of the dual-mode DWR, it also increases the coupling intensity between mode 1 and 2. However, because required cross-coupling intensity is relatively weak, the cross-coupling slot for k_{13} is usually small. Thus it has limited influence on the coupling intensity of k_{12}.

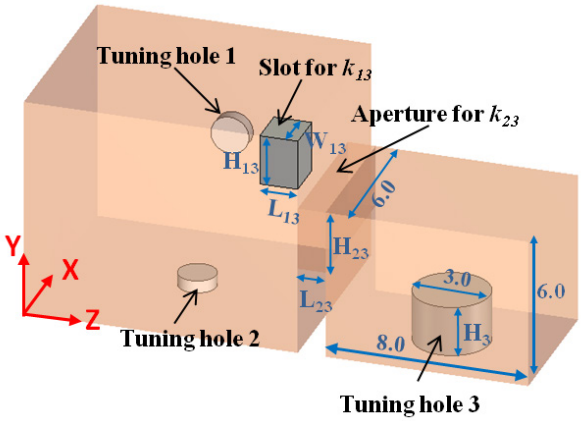

Figure 3. Inter-resonator coupling structure.

The simulated coupling coefficients are presented in Figure 4. When obtaining k_{23}, mode 1 is detuned to 4.4 GHz and the dimensions are: $\boldsymbol{H}_1$=1.8 mm, $\boldsymbol{H}_2$=0.5 mm, $\boldsymbol{H}_3$=2 mm, and $\boldsymbol{L}_{23}$=1.1 mm. When obtaining k_{13}, mode 2 is detuned to 4.4 GHz and the dimensions are: $\boldsymbol{H}_1$=0.5 mm, $\boldsymbol{H}_2$=1.8 mm, $\boldsymbol{H}_3$=1.9 mm, $\boldsymbol{L}_{23}$= 1.1 mm, $\boldsymbol{H}_{23}$= 3 mm and $\boldsymbol{L}_{13}$= 1.5 mm.

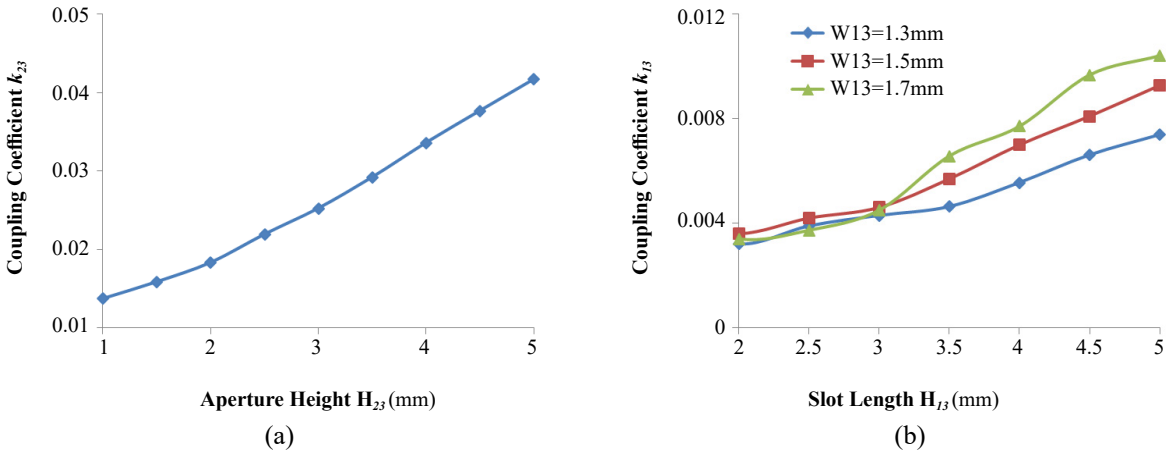

Figure 4. Simulated inter-resonator coupling coefficients. (a) For k_{23}. (b) For k_{13}.

The external coupling structure for mode 1 is shown in Figure 5(a), formed by a silver-coated blind hole and an uncoated port area. The external Q-factors were simulated against the radius of shielded area and the depth of input hole. During simulation, mode 2 was detuned with dimensions $\boldsymbol{H}_1$=0.5 mm, $\boldsymbol{H}_2$=1.8 mm. Figure 5(b) shows the simulated external Q-factors, where the input hole depth $\boldsymbol{H}_{in}$ plays a dominant role controlling the intensity of external coupling.

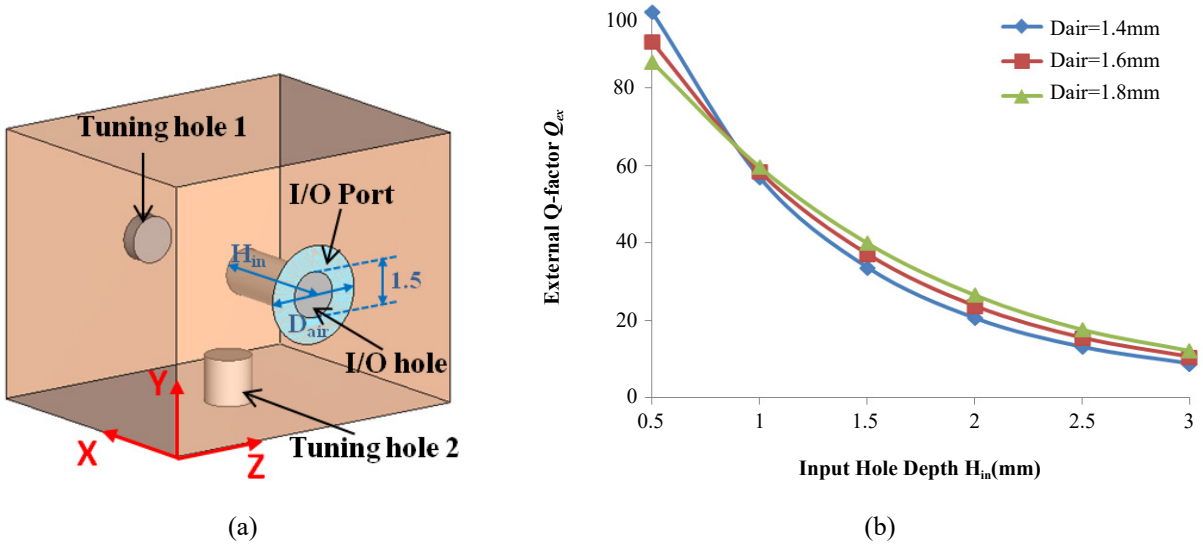

Figure 5. External coupling structure and simulated external Q-factor. (a) Structure. (b) Simulated Q_{ex}.

2.3 *Transmission Zero Analysis*

Figure 6 shows the E-fields of the modes with coupling slot positions at the top and the bottom on XY plane. The resonant frequencies have minor change since the coupling is slightly influenced by the position of slot. Nevertheless, changing the relative position of coupling slot interchanges the resonant frequencies of the original TE_{101} and TE_{011} mode. This means a coupling type change for k_{12}. Therefore, the relative position of the inter-mode coupling slot can be used to adjust TZ to above or below filter passband.

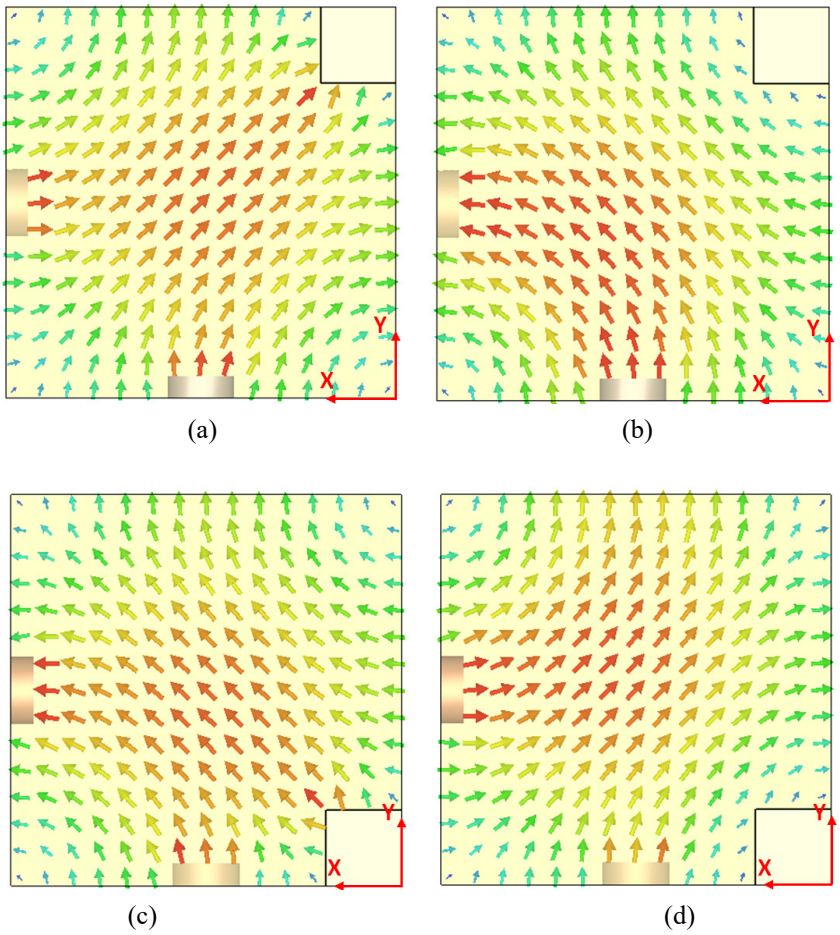

Figure 6. E-field of resonant modes with different slot position. (a) Original TE_{011} mode at 4.861 GHz. (b) Original TE_{101} mode at 5.053 GHz. (c) Original TE_{101} mode at 4.864 GHz. (d) Original TE_{011} mode at 5.068 GHz.

Figure 7 shows a three-pole filter with a TZ above passband. The coupling topology and coupling coefficients are shown in Figure 7(b). The dimensions are: H_1=0.28, H_2=0.47, H_3=1.84, H_{in}=2.15, H_{out}=2.05 and D_{air}=3.2 (Unit: mm), where H_{in} and H_{out} denote depth of input and output holes, D_{air} represents the diameter of I/O port, respectively.

Figure 8 shows another filter with similar passband. The coupling coefficients in Figure 8(b) are very close to those in Figure 7(b), except for the frequency offset of resonant modes. By changing the coupling slot position of k_{12}, the resonant frequencies of mode 1 and 2 are swapped. Then the TZ is translated to lower stopband. The filter dimensions are: H_1=0.5, H_2=0.4, H_3=1.84, H_{in}=2.78, H_{out}=2.08 and D_{air}=3.2 (Unit: mm).

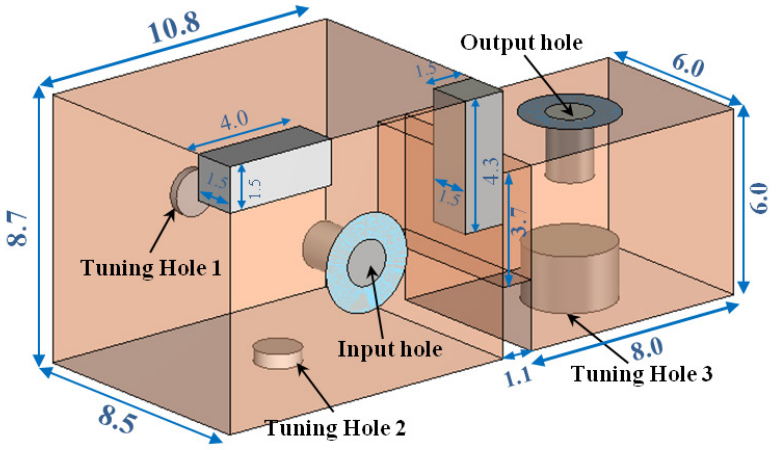

(a)

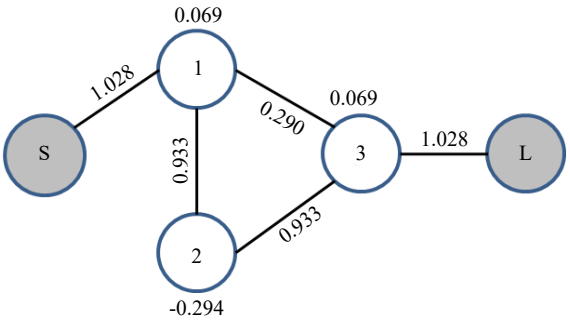

(b)

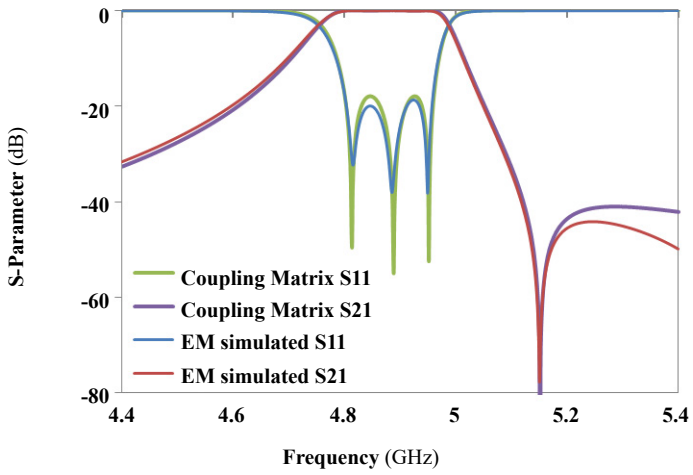

(c)

Figure 7. Filter with a TZ above passband. (a) Filter structure. (b) Coupling topology. (c) Simulated frequency response.

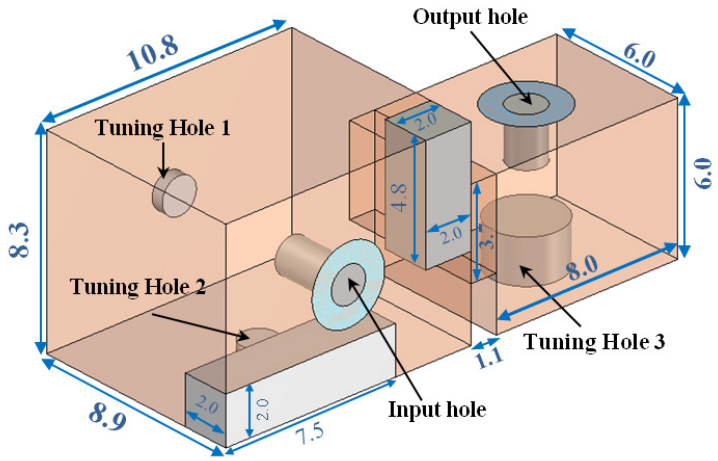

(a)

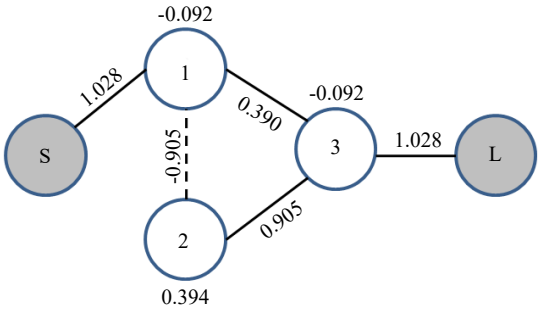

(b)

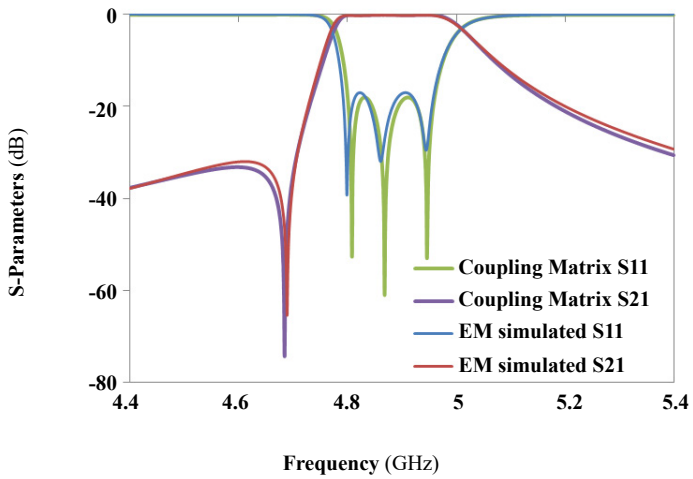

(c)

Figure 8. Filter with a TZ below passband. (a) Filter structure. (b) Coupling topology. (c) Simulated frequency response.

3. Filter Design and Implementation

A sixth order bandpass filter working at band N79 is designed. The specifications are: Centre frequency f_0=4.9GHz, bandwidth BW=160MHz, return loss RL≤−18 dB.

Figure 9 shows the filter topology and synthesized coupling coefficients. The filter composes of two dual-mode DWRs and two single-TE_{101}-mode DWRs. Each CT coupling topology generates a TZ at stopband.

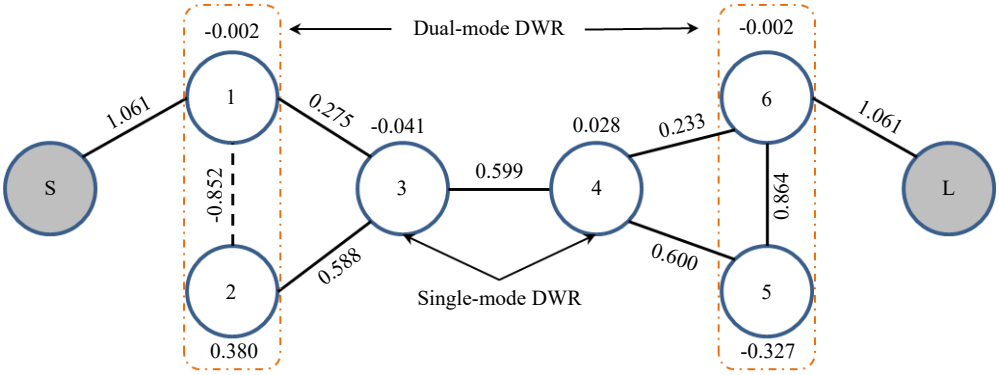

Figure 9. Topology and coupling coefficients of the six-pole BPF.

Figure 10 shows the designed filter model. For practice, the inter-resonator coupling apertures are blended with a radius of 0.5 mm and the filter edges are blended or chamfered by 0.3 mm. The dimensions were initially set according to coupling profiles and filter models in above sections, and then optimized in EM simulation. During simulation, the conductivity of silver coating and background is set as 3e7 S/m. Other optimized dimensions are as follows: $\boldsymbol{H_1}$=0.84, $\boldsymbol{H_2}$=1.05, $\boldsymbol{H_3}$=1.97, $\boldsymbol{H_4}$=1.96, $\boldsymbol{H_5}$=1.44, $\boldsymbol{H_6}$=0.91, $\boldsymbol{H_{in}}$=2.3, $\boldsymbol{H_{out}}$=2.85, $\boldsymbol{D_{in}}$=$\boldsymbol{D_{out}}$=1.2 and $\boldsymbol{D_{air}}$=3.24 (Unit: mm).

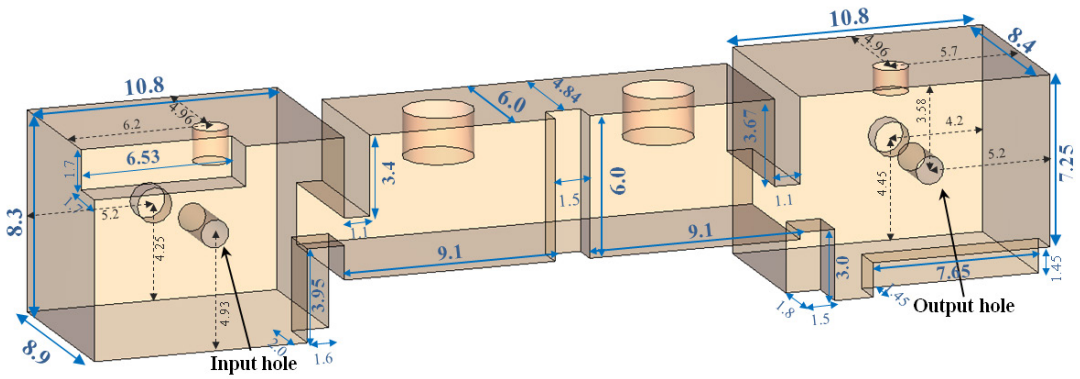

Figure 10. EM model and dimensions of the designed filter.

The designed filter is made of a formed and sintered ceramic monoblock. Holes and slots are machined and milled. Then the outer-surfaces of ceramic block are metalized using silver-spraying and silver-sintering process. The silver-coating at ring areas around I/O holes are removed by laser engraving. The filter is tuned, shown in Figure 11. During tuning process, removing the silver-coating on the sidewalls of tuning holes results in frequency decrease. To increase

the resonant frequency, the silver-coating on bottom surface of holes and the surface with tuning holes need to be partly removed. Removing the silver at the coupling slots and apertures will decrease the coupling intensity

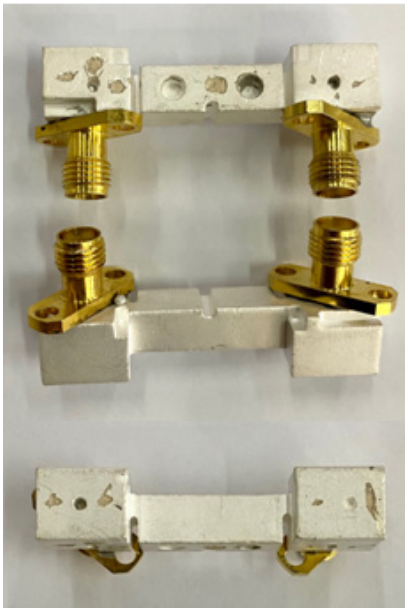

Figure 11. Photograph of the fabricated filter.

Figure 12 presents the simulated and the measured frequency responses. The difference is caused by the material discrepancy on dielectric constant and silver conductivity, and dimension tolerances of the filter. The proposed dual-mode DWR, coupling structures and TZ analysis are validated by the good agreement between measurement and simulation.

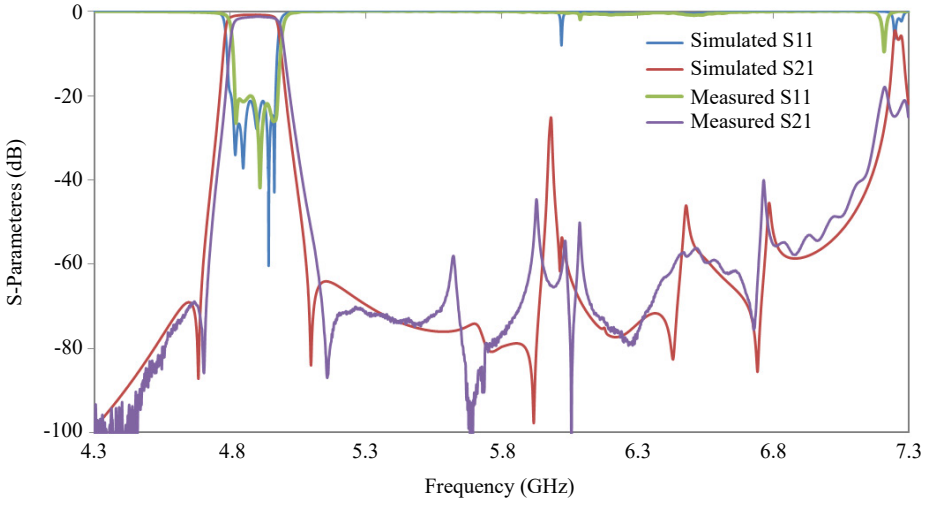

(a)

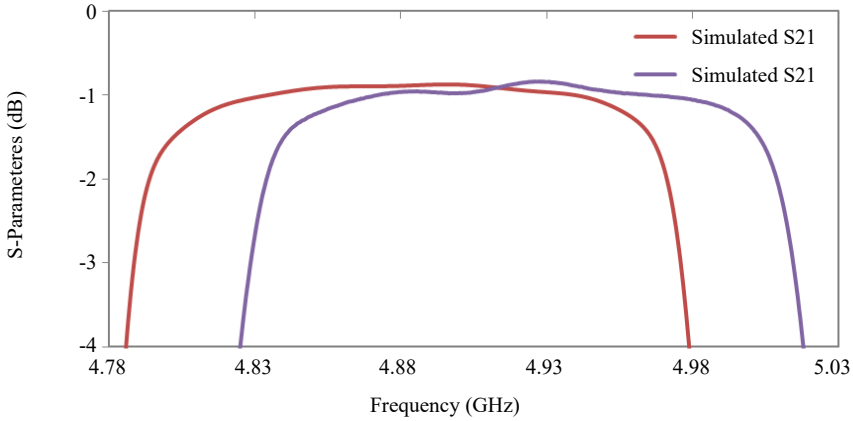

Figure 12. Simulated and measured frequency responses. (a) Wideband responses. (b) The passband.

4. Conclusions

In this paper, a dual-mode DWR structure has been proposed for compact filter design. The dual-mode DWR offers relatively high Q-factor in a small volume. The inter-mode coupling can be easily realized by slots on the dielectric block. The in-line coupling and cross coupling between a dual-mode DWR and a single-mode DWR are realized and controlled by a dielectric aperture and a silver-coated slot. When cascading the dual- and single-mode DWR for filter design, the frequency position of TZ can be adjusted to low- or high-stopband by changing the relative position of the dual-mode coupling slot. A sixth order bandpass filter is designed and implemented using dual- and single-mode DWRs. The filter has a compact size, low-loss, good selectivity and wide spurious-free response, which is suitable for application of 5G band N79 base stations.

Acknowledgments

The authors express their thanks to the people helping with this work, and acknowledge the valuable suggestions from the peer reviewers.

Conflict of Interest

There is no conflict of interest for this study.

References

[1] Bjornson, E.; Van der Perre, L.; Buzzi, S.; Larsson, E.G. Massive MIMO in Sub-6 GHz and mmWave: Physical, Practical, and Use-Case Differences. *IEEE Wirel. Commun*. **2019**, 26, 100–108, https://doi.org/10.1109/mwc.2018.1800140.

[2] Hong, W.; Jiang, Z.H.; Yu, C.; Zhou, J.; Chen, P.; Yu, Z.; Zhang, H.; Yang, B.; Pang, X.; Jiang, M.; et al. Multibeam Antenna Technologies for 5G Wireless Communications. *IEEE Trans. Antennas Propag*. **2017**, 65, 6231–6249, https://doi.org/10.1109/tap.2017.2712819.

[3] Sano, K.; Miyashita, M. Dielectric waveguide filter with low profile and low-insertion loss. *IEEE Trans. Microw. Theory Tech*. **1999**, 47, 2299–2303, https://doi.org/10.1109/22.808974.

[4] Cameron, R.; Rhodes, J. Asymmetric Realizations for Dual-Mode Bandpass Filters. *IEEE Trans. Microw. Theory*

Tech. **1981**, 29, 51–58, https://doi.org/10.1109/tmtt.1981.1130286.
[5] Yassini, B.; Yu, M. Ka-Band Dual-Mode Super Q Filters and Multiplexers. *IEEE Trans. Microw. Theory Tech*. **2015**, 63, 3391–3397, https://doi.org/10.1109/tmtt.2015.2462822.
[6] Bastioli, S.; Tomassoni, C.; Sorrentino, R. A New Class of Waveguide Dual-Mode Filters Using TM and Nonresonating Modes. *IEEE Trans. Microw. Theory Tech*. **2010**, 58, 3909–3917, https://doi.org/10.1109/tmtt.2010.2086068.
[7] Gerini, G.; Bustamante, F.D.; Guglielmi, M. Triple mode filters with coaxial excitation. In Proceedings of 2000 IEEE MTT-S International Microwave Symposium Digest (Cat. No.00CH37017), Boston, MA, USA, 11–16 June 2000.
[8] Fiedziuszko, S. Dual-Mode Dielectric Resonator Loaded Cavity Filters. *IEEE Trans. Microw. Theory Tech*. **1982**, 30, 1311–1316, https://doi.org/10.1109/tmtt.1982.1131253.
[9] Walker, V.; Hunter, I. Design of triple mode TE01spl delta// resonator transmission filters. *IEEE Microw. Wirel. Components Lett*. **2002**, 12, 215–217, https://doi.org/10.1109/lmwc.2002.1009999.
[10] Accatino, L.; Bertin, G.; Mongiardo, M.; Resnati, G. Dual-mode filters with grooved/splitted dielectric resonators for cellular-radio base stations. *IEEE Trans. Microw. Theory Tech*. **2002**, 50, 2882–2889, https://doi.org/10.1109/tmtt.2002.805286.
[11] Rahman, M.M.; Wang, W.; Wilber, W.D. A compact triple-mode plated ceramic block based hybrid filter for base-station applications. In Proceedings of 34th European Microwave Conference, Amsterdam, Netherland, 12–14 October 2004.
[12] Chen, Y.; Zhang, Y.; Wu, K.-L. A Dual-Mode Monoblock Dielectric Bandpass Filter Using Dissimilar Fundamental Modes. *IEEE Trans. Microw. Theory Tech*. **2021**, 69, 3811–3819, https://doi.org/10.1109/tmtt.2021.3089720.
[13] Wu, Y.; Jin, L.; Lu, Z. A Triple-Quasi-TEM-Resonance Dielectric Cavity for Bandpass Filter Design. *IEEE Microw. Wirel. Components Lett*. **2022**, 32, 950–952, https://doi.org/10.1109/lmwc.2022.3163757.
[14] Chu, Q.-X.; Mai, J.-Y.; Shu, P.-W. Novel Dual-Mode Dielectric-Filled Waveguide Filters. In Proceedings of 2020 IEEE Asia-Pacific Microwave Conference (APMC), Hong Kong, China, 8–11 December 2020.
[15] Huang, Z.; Cheng, Y.; Zhang, Y. Dual-Mode Dielectric Waveguide Filters with Controllable Transmission Zeros. *IEEE Microw. Wirel. Components Lett*. **2021**, 31, 449–452, https://doi.org/10.1109/lmwc.2021.3064088.
[16] Zhu, Y.-Y.; Chen, J.-X. Novel Differential Dielectric Waveguide Filter Using Spatial Coupling Mechanism. IEEE *Microw. Wirel. Components Lett*. **2017**, 27, 971–973, https://doi.org/10.1109/lmwc.2017.2750025.
[17] Meng, S.; Liang, F.; Lin, Z.; Lu, W.; Wang, X. Design of Six-cavity Ceramic Waveguide Filter with Four Transmission Zeros. In Proceedings of 2021 IEEE 4th International Conference on Electronic Information and Communication Technology (ICEICT). Xi'an, China, 18–20 August 2021.